ACS APPLIED MATERIALS & INTERFACES

Letter

www.acsami.org

Highly Stretchable and Sensitive Unidirectional Strain Sensor via Laser Carbonization

Rahim Rahimi, Manuel Ochoa, Wuyang Yu, and Babak Ziaie*

Birck Nanotechnology Center and School of Electrical and Computer Engineering, Purdue University, West Lafayette, Indiana 47907, United States

Supporting Information

ABSTRACT: In this paper, we present a simple and low-cost technique for fabricating highly stretchable (up to 100% strain) and sensitive (gauge factor of up to 20 000) strain sensors. Our technique is based on transfer and embedment of carbonized patterns created through selective laser pyrolization of thermoset polymers, such as polyimide, into elastomeric substrates (e.g., PDMS or Ecoflex). Embedded carbonized materials are composed of partially aligned graphene and carbon nanotube (CNT) particles and show a sharp directional anisotropy, which enables the fabrication of extremely robust, highly stretchable, and unidirectional strain sensors. Raman spectrum of pyrolized carbon regions reveal that under optimal laser settings, one can obtain highly porous carbon nano/microparticles with sheet resistances as low as 60 Ω/□. Using this technique, we fabricate an instrumented latex glove capable of measuring finger motion in real-time.

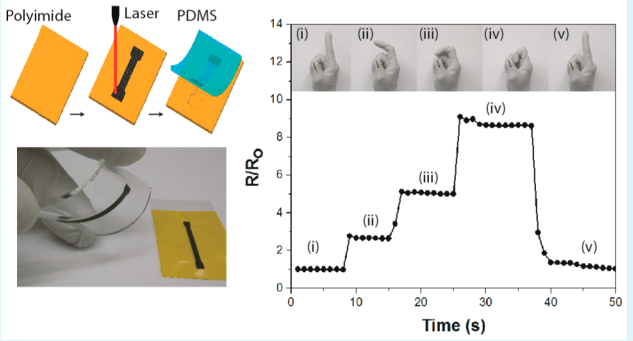

KEYWORDS: *carbonization, pyrolysis, piezoresistance, stretchable, laser, gauge factor, strain sensor*

Stretchable and flexible sensors have attracted considerable attention for their potential applications in wearable electronics,[1] smart textiles,[2] soft robotics,[3] and structural health monitoring.[4] Among the various types of transducers available for these applications, piezoresistive strain sensors are among the most investigated ones. These are often used for human motion analysis in applications such as athletic assessments,[5] kinesiology, and interactive entertainment systems.[6] Traditional metallic and semiconducting strain sensors are not suitable for stretchable applications because they can only withstand very limited strain (<5%) before fracture.[7,8] Today's most common approaches for fabrication of highly stretchable piezoresistive[9] and piezocapacitive[10,11] strain sensors are based on two main techniques: (1) conductive-liquid-filled elastomeric tubes or microchannels,[12] and (2) polymeric blends or composites prepared by embedding conductive nanomaterials within an elastomeric network.[13,14] The first method dates back to 1953 when Whitney used mercury-filled elastomeric tubes to measure blood volume in the limbs (mercury-in-rubber plethysmograph).[15] When strained, the tube was stretched and narrowed, resulting in an increased resistance, forming a low-cost piezoresistive sensor. More recently, several groups have reported on miniaturized variations of this technique using microchannels filled with eutectic gallium–indium[16,17] or carbon grease.[18] Despite its attractive simplicity, this method suffers from various drawbacks, including small gauge factor, leakage of the liquid upon strain (mostly at the electrical connections ends), and technical challenges associated with filling a highly viscous fluid into microchannels. The second method relies on making elastomeric composites containing conductive nanomaterials (e.g., carbon nanotubes,[9] graphene,[19,20] silver nanowires[21]) that are either embedded directly into the elastomeric material[22,23] or deposited on the surface of a stretchable substrate using various methods such as contact transfer printing,[24] screen printing,[25] and inkjet printing.[26−28] Recent examples of the latter method include screen printing of silver nanowire networks onto glass slides that are subsequently transferred to an elastic matrix[21] and mixing graphene with cellulose nanoparticles in a controlled ratio to create stretchable conductive nanopaper.[29] Despite their promising performance, these techniques pose various practical fabrication challenges. For instance, making CNT and conductive nano particles for use in these processes requires time-consuming and complex synthesis, often in a clean room facility, which increases the overall cost of and limits the scalability of the process. Many also require aligned single-walled carbon nanotube (SWCNT) thin films which are difficult to grow controllably and must often be transferred manually onto the stretchable substrate.[9] Additionally, depositing and uniformly dispersing the nanoparticles by inkjet printing and screen printing is also challenging; the nanoparticles tend to aggregate, requiring additional processing steps

Received: December 25, 2014
Accepted: February 16, 2015
Published: February 16, 2015

DOI: 10.1021/am509087u
ACS Appl. Mater. Interfaces 2015, 7, 4463−4470

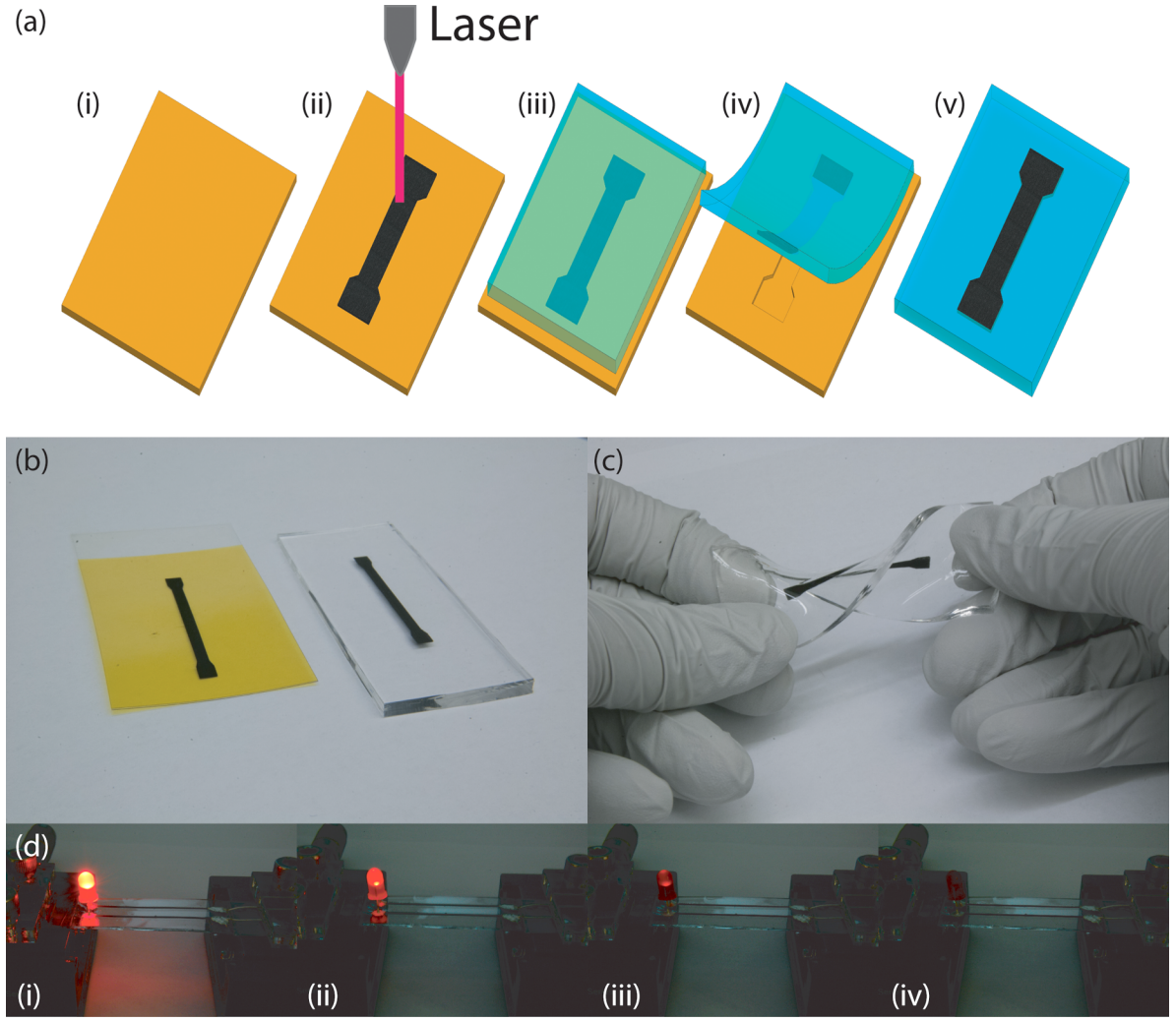

Figure 1. (a) Schematic of the fabrication process for stretchable carbon nanocomposite using laser pyrolization of polyimide: (i) attach polyimide tape to a PET sheet; (ii) laser-carbonize patterns on the polyimide; (iii) pour and impregnate carbon traces with diluted uncured PDMS; (iv, v) peel off the PDMS sheet after cross-linking. (b) Carbon trace before and after transferring to the PDMS. (c) Twisted carbon trace. (d) Lit LED connected to carbon traces showing diminished brightness as a function of strain: (i) 0, (ii) 2, (iii) 4, and (iv) 6%.

to ensure uniform dispersal (e.g., using surfactants and sonication).

As an alternative approach addressing some of the above-mentioned problems, we present a simple and low-cost technique (with a cost of $ 20 per m^2) to create highly stretchable (up to 100% strain) and sensitive (gauge factor of up to 20 000) strain sensors using laser-carbonized nanomaterials. The stretchable strain sensors consist of PDMS embedded with patterns of partially aligned mico/nano carbon particles. The carbon nanomaterials are created by direct laser-pyrolization of a polyimide tape, resulting in highly porous carbon traces. The carbon particles are subsequently transferred to and encapsulated within an elastomeric material, yielding highly stretchable and unidirectional piezoresistive strain sensors (the same method can be used to fabricate piezocapacitive sensors).

Figure 1a illustrates the fabrication process of the stretchable carbon traces. First, a piece of polyimide tape is attached to a PET sheet to provide handling rigidity during the process (Figure 1a.i). Next, a CO_2 laser engraving system (PLS6MW, Universal Lasers, Inc., Scottsdale, AZ) is used to inscribe highly porous carbon patterns in the desired shape on the surface of the polyimide tape (Figure 1a.ii). This is achieved by locally pyrolizing the surface of the polymer into carbon nanomaterials (e.g., CNTs, graphene). The traces are subsequently immersed in *n*-heptane for 20s; this improves the adhesion and increases the penetration of the elastomeric materials into the carbon network. In order to make stretchable sensors, the carbon patterns are then transferred to polydimethylsiloxane (PDMS). This is accomplished by pouring a diluted form of uncured PDMS (prepolymer with 7% n-heptane) over the carbon patterns, followed by degassing and cross-linking (at 70 °C for 2 h) (Figure 1a.iii). The use of diluted prepolymer results in improved impregnation of the carbon patterns with PDMS during the vacuum degassing step. After cross-linking, the PDMS is peeled off the polyimide substrate (Figure 1a.iv-v). Figures 1b, c shows photographs of the carbon patterns before and after transfer to the PDMS substrate. Figure 1d, e shows an LED attached to a 3 V battery through two parallel carbon traces of 1 mm width and 3 cm length. In an unstrained state, the LED is brightly lit, whereas at low strain levels (5%), the LED begins to dim. At higher strains (>5%), the conductivity of the traces decreases significantly until the LED is eventually turned off.

DOI: 10.1021/am509087u
ACS Appl. Mater. Interfaces 2015, 7, 4463−4470

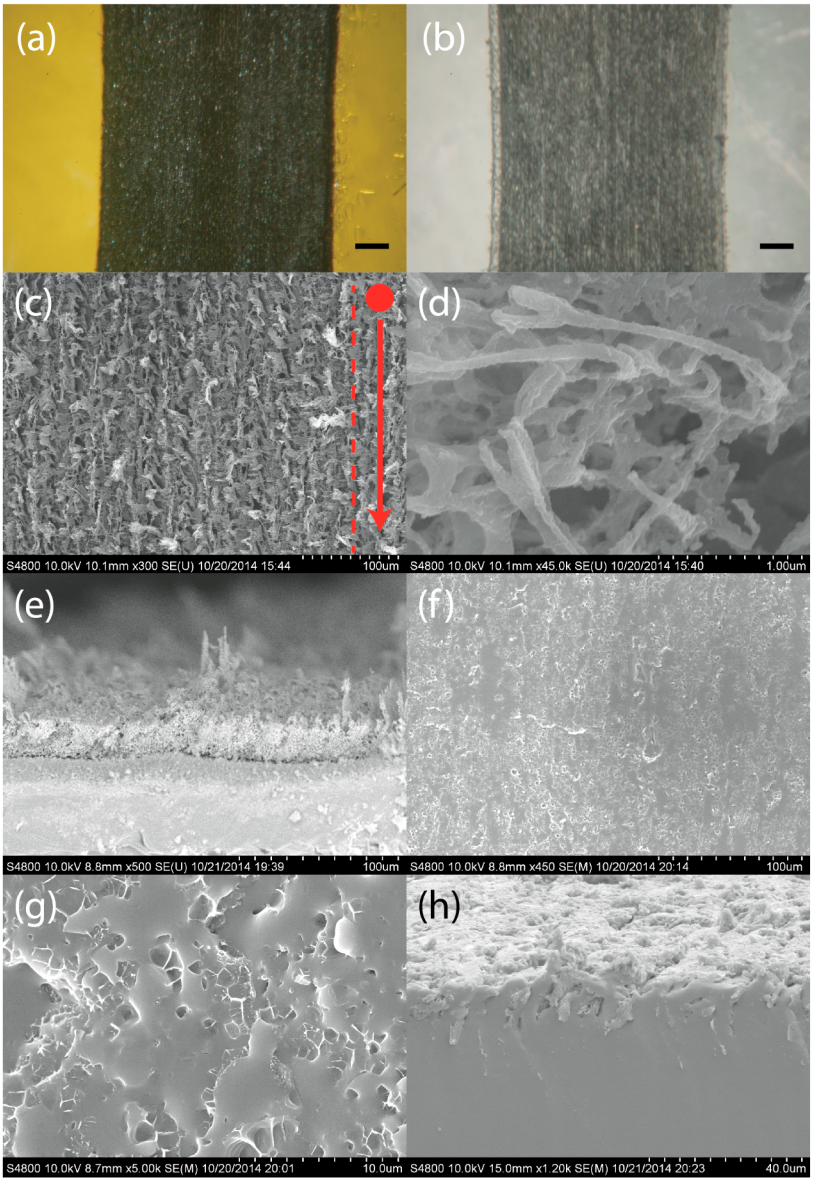

Figure 2. Surface and film architecture details. (a, b) Optical images of the carbonized polyimide before and after transfer to the PDMS. Scale bar 250 μm. (c) SEM image of the aligned particles in the traces with the arrow showing the direction of laser ablation. (d) High-magnification SEM image showing nanoparticles and fibers. (e) Cross-section image of the carbon traces showing the porosity of the carbonized material. (f, g) SEM images of the carbon particles after transfer to the PDMS at different magnifications. (h) Cross-section SEM of stretchable carbon traces embedded in PDMS.

The surface morphology of the carbon patterns, before and after embedment in the PDMS, was qualitatively investigated by scanning electron microscopy (SEM) (Figure 2). The top view of carbon traces clearly reveals highly porous carbon micro- and nanoparticles arranged in a parallel pattern. This phenomenon is related to the method by which the laser beam is scanned across the sample during the fabrication. Since the spot size (diameter) of the laser beam in our system is 60 μm, ablation of areas larger than 60 μm requires multiple sweeps of the laser beam over the targeted area; thus generating carbon particles in a parallel orientation to the direction of laser motion. Higher magnified pictures of the carbon particles in the pyrolized lines are shown in Figure 2c, d. Partially oriented carbon flakes and high-aspect-ratio filaments (some of them as small as ~70 nm wide with lengths of up to ~2 μm) can be seen on the carbon traces. A cross-sectional view of the carbon patterns shows that the entire thickness of the pyrolized carbon is comprised of highly porous nanomaterials. This enables the PDMS to penetrate deep into the carbon patterns (Figure 2e), resulting in a uniform transfer of carbon nanoparticles to the elastomeric matrix (Figures 2f, g). The thickness of the carbonized regions embedded in the PDMS is ~30 μm (Figure 2h), which is close to their original thickness on the polyimide (before transfer). The microstructure quality of the carbon nanomaterials was evaluated by transmission electron microscopy (TEM). The samples were prepared by cutting the carbonized layer to a thickness of 100 nm using an ultramicrotome and placed on a copper grid. TEM images reveal the presence of multiple layers of oriented CNTs with widths as small as 40 nm (see Figure S1 in the Supporting Information).

DOI: 10.1021/am509087u
ACS Appl. Mater. Interfaces 2015, 7, 4463−4470

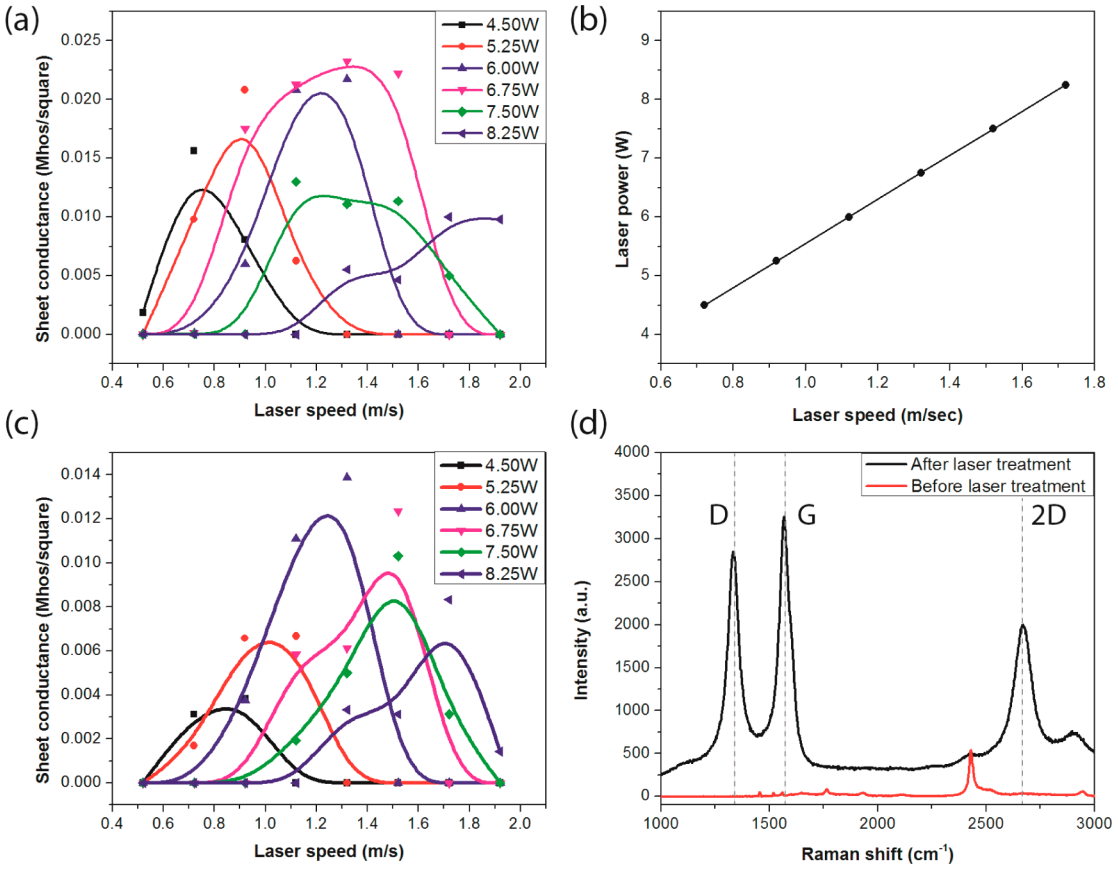

Figure 3. Electrical characterization of pyrolized carbon patterns. (a) Sheet conductivity of carbon trace on polyimide as a function of laser fabrication parameters (power and speed). (b) Power and speed required to achieve carbon traces with high sheet conductivity (low sheet resistance). (c) Sheet conductivity of carbon trace after transfer to the PDMS as a function of laser fabrication parameters (power and speed). (d) Raman spectra before and after laser treatment showing the appearance of D,G and 2D peaks 1350, 1580, and 2700 cm^{-1}, respectively.

The electrical conductivity of the carbon patterns before and after transfer to the elastomeric matrix was measured by four-point-probe technique. Figure 3 demonstrates the sheet conductivity of the carbon patterns as a function of the fabrication parameters, i.e., speed and power of the laser, before and after transfer to the PDMS. The plots show the strong dependence of the sheet conductivity on both power and speed of the laser. In practice, the polyimide can be carbonized with the laser once the polymer reaches the threshold energy needed to initiate the pyrolization process (this also results in a weight reduction of the pyrolized polymer, polyimide). As the plots show, the threshold energy can be achieved at different laser powers and speeds. For example, with lower laser speeds, carbonization occurs at low power levels, whereas with higher laser speeds, carbonization requires a higher power. We observed that when the thermal energy is too large (laser power >8.25 W and raster speed <1.0 m/s) the polymer turns into a white ash and exhibits a mass reduction of about 90%, but when the thermal energy is too low (laser power <4.5 W and raster speed >1.5 m/s), the polymer does not carbonize and shows a negligible change in the mass, both phenomena resulting in a low conductivity. Figure S2 in the Supporting Information shows the change in the mass of the polymer after laser carbonization on a surface of 7 mm × 7 mm using different laser parameters (speed and power).

The Gaussian shape of the conductivity plots in Figure 3a reflects this behavior, showing that there is an optimum combination of laser power (4.5 to 8.25 W) and speed (0.5 m/s to 1.9 m/s) needed for producing high-quality, high-conductivity traces. The optimal setting corresponds to the maxima at each plot; these are plotted in Figure 3b, showing a linear relationship with speed and power (a maximum conductivity of 0.02 Mhos/□ with 6.75 W and 1.3 m/s). The slope of the plot shows the optimal energy density (62 000 J/m^2) needed to achieve low resistance carbon traces. Laser ablations with energy densities below or above this threshold will result in either insufficient energy for complete carbonization or burning of the polymer, respectively. The carbon patterns exhibit a small dip in conductivity after transfer to the PDMS; this decrease can be attributed to an incomplete transfer where residual amounts of carbon particles remain on the polyimide surface (Figure 3c).

The structural characteristics of the carbon nanomaterials were studied via Raman spectroscopy. Figure 3d shows the Raman spectra recorded from the center of the carbon patterns in the range of 1000−3000 cm^{-1} using an excitation laser source at 532 nm. The data clearly show three distinctive Raman spectra peaks at 1350 cm^{-1} (D-band), 1580 cm^{-1} (G-band), and 2700 cm^{-1} (2D-band) after laser carbonization, which suggest the presence of CNT and graphite in the carbonized material. The peak located at 1580 cm^{-1} (G-band) is the primary phonon arising from lattice stretching in the C−C bonding in the graphitic plane. The D-band observed at about 1350 cm^{-1} corresponds to the disorder and defects in the graphitic lattice. The ratio of the peak intensity (I_D/I_G) of the D and G bands is a parameter used to quantify the amount of

DOI: 10.1021/am509087u
ACS Appl. Mater. Interfaces 2015, 7, 4463−4470

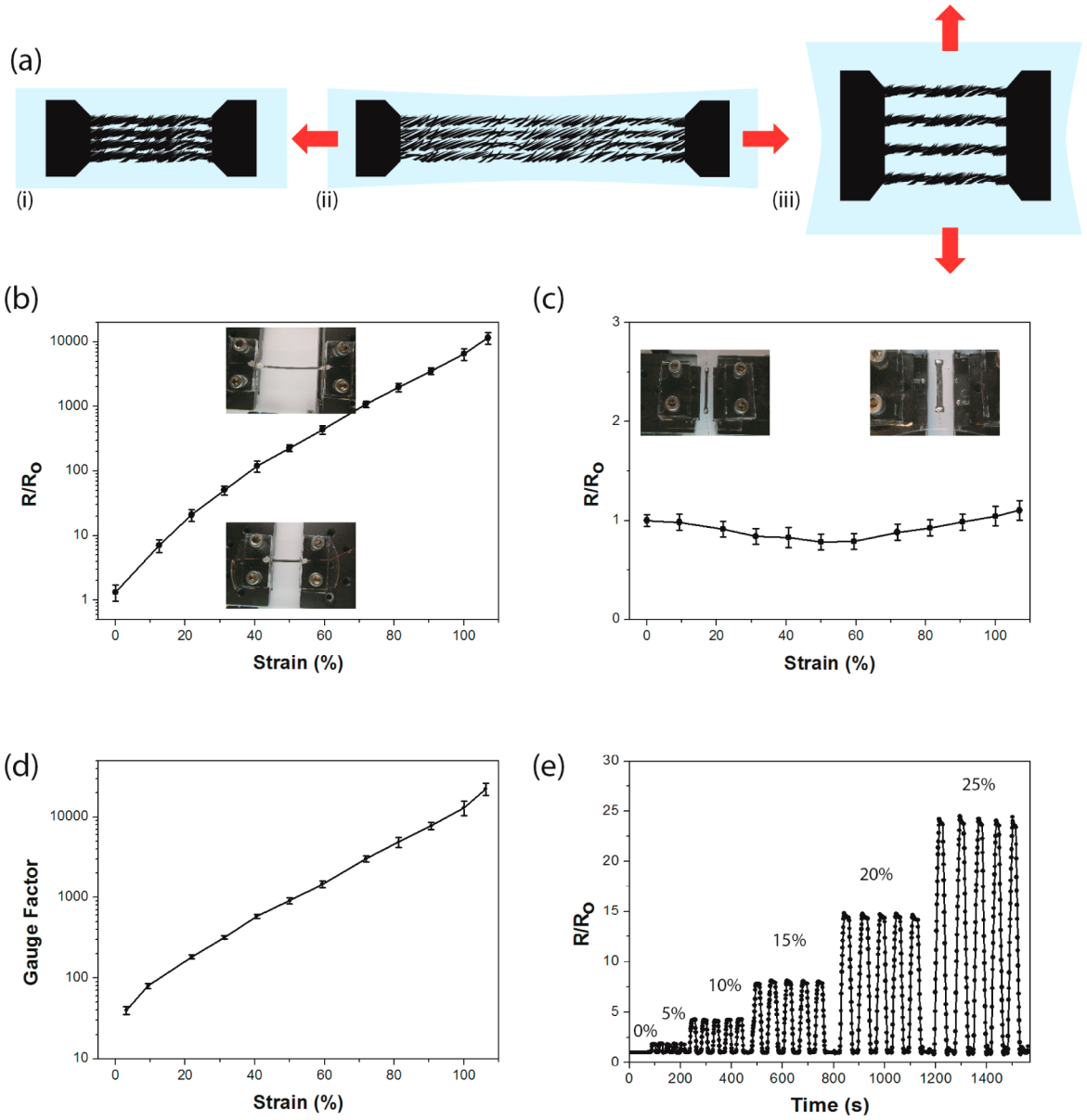

Figure 4. Characterization of the stretchable carbon traces subjected to longitudinal and transverse strain. (a) Illustrations of carbon traces (i) in their relaxed state, (ii) under longitudinal strain, and (iii) under transverse strain. (b) Plot of the relative resistance change for different levels of longitudinal strain. (c) Plot of the relative resistance change for different levels of transverse strain. (d) Gauge factor of the stretchable carbon traces versus longitudinal strain. (e) Dynamic stretch-and-release cycle response of the sensor for various strains 0−25%.

defects in the graphitic material. The I_D/I_G (~0.8) ratio analyzed form the Raman spectra shows a reasonable amount of defect in the graphitic materials.[30] The 2D band is due to a secondary phonon vibration of the C−C bonding. This band provides information about stacking layers in the carbonized material (such as CNT, graphene). The ratio between the 2D and G bands ($I_{2D}/I_G \approx 0.7$) calculated for the Raman data indicates that the graphitic material is composed of mostly three carbon layers.[31,32]

The performance of several prototype strain sensors consisting of four traces each 2 mm wide and 30 mm long was evaluated at room temperature by continuously recording the change in the resistance while the device was stretched by a micromanipulator. To ensure reliable electrical connections, we applied silver paste on the two ends of the device. The baseline resistance of the device (unstrained) was ~1 kΩ, comparable to the reported piezoresistive strain sensors made with CNT (~100 Ω) and AgNW (~250 Ω) composites.[21] Figure 4a shows a series of pictures depicting the sensor under longitudinal (length) and transverse (width) strain. Unlike other composites in which the conductive nanoparticles are isotropically dispersed and oriented, the particles in our patterns possess an anisotropic orientation due to the above-mentioned laser rastering process. This results in sensors with unidirectional sensitivity, i.e., conductivity is strongly affected by the longitudinal strain, whereas remains essentially constant under transverse strain. The application of longitudinal strain increases the spacing between the conductive particles and lowers the number of contact points between the particles, resulting in an increased resistance. On the other hand, the number of contact points between the carbon particles does not change significantly when the device is stretched in the

DOI: 10.1021/am509087u
ACS Appl. Mater. Interfaces 2015, 7, 4463−4470

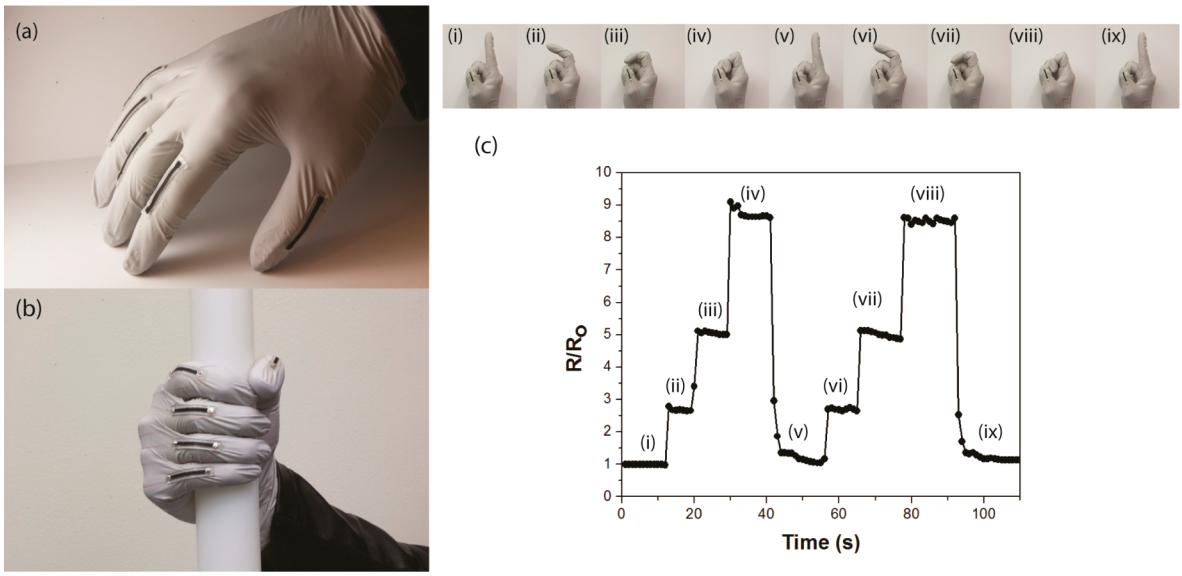

Figure 5. Human finger motion detection with stretchable carbon traces. (a, b) Photograph of five stretchable strain sensors attached to the finger joints on the glove. (c) Relative resistance change of the strain sensors at different bending stages over time; the corresponding finger configuration for each plot region i–ix is shown in the snapshots below the plot.

transverse direction. Figure 4b, c illustrates the relative change in resistance in response to the applied strain for five samples. The device exhibits a very large change in resistance (>20 MΩ) for 100% longitudinal strain, Figure 4b, but its resistance changes negligibly (~100 Ω) in response to 100% transverse strain, Figure 4c. The smaller decrease in the resistance for strain levels of <40% (Figure 4b) can be attributed to the Poisson effect, which results in higher particle density in the middle of the trace (more contact points and increased conductivity). In both cases, the device showed no signs of failure for up to 100% strain. Further stretchability is limited by the elastomeric properties of the PDMS substrate; however, this can be extended by using a more elastic material such as Ecoflex. The unidirectionality of such sensors makes them suitable for applications that require strain direction detection; for example, an orthogonal arrangement of three such sensors can form a coordinate system for measuring strain in three-dimensional space.

For comparison to other reported stretchable strain sensors, we calculated the gauge factor ($G = (R/R_0)/(\Delta L/L)$) of our device from the measured data for both longitudinal and transverse strains. Figure 4d shows the longitudinal gauge factor (semilog plot) as a function of strain. The exponential change in the gauge factor at higher strain levels is attributed to the drastic change in resistance at higher levels of longitudinal elongation (gauge factor of 50 at 5% strain to a gauge factor of 20 000 at 100% strain). This high gauge factor is significantly larger than those reported for conductive composites as well as metal strain gauges. The state-of-the-art graphene-based composites typically exhibit gauge factors within the range of 2–50, whereas CNTs and AgNWs sensors have an even smaller gauge factors 1–7.[20,28] Although the variable gauge factor values of our device may require additional logarithmic circuitry for linearization, the increased sensitivity to high strain levels makes it ideal for human body applications where detecting higher strain levels is often more critical.

The performance stability of the sensor was evaluated by subjecting it to 1000 stretch-and-release cycles (0–100% strain). Figure S3a (Supporting Information) shows the resistance change in response to longitudinal strain after different numbers of cycles. After 1000 cycles, the maximum drift in strain was 3% (at the lowest resistance), acceptable for many biomedical applications. This change can be attributed to migration or rearrangement of the conductive nanoparticles in the polymer matrix, thus altering the original alignment.

To assess the dynamic performance of the device, we subjected the sensors to different levels of strain while their resistance was continuously measured. Figure 4e shows the results of five stretch-and-release cycles for strain levels of 0–25%. The sensor shows a fast response (<1 s) to the applied strain as well as a full recovery upon release. To evaluate the transient stability, we investigated its stress relaxation behavior by subjecting the sensor to steps of 10% strain from 0 to 100%. For each step, the sensor was stretched 10% and held at that position for 3 min while the resistance was continuously monitored. The results are plotted in Figure S3b of the Supporting Information. For strain levels in the range 0–50% the sensor exhibits a fast response with overshoots of less than 4%. Such values are comparable to some of the highest-performance piezoresistive sensors reported in the literature (i.e., about 3% overshoot and 5 s response time).[9] For strain levels above 50%, our sensor shows larger overshoots (~7%) and stabilization time (~25 s); these values, while higher, are still sufficiently fast for many practical applications, especially with respect to biological kinetics (e.g., wound healing or muscle repair) and human motion. In such applications, the performance of our sensor exceeds that of many other previously reported piezoresistive conductive composites and thin conductive-particle films, many of which lack long-term stability, suffer from high overshoots (~9%), and require long recovery time (~100 s).[1]

To demonstrate the utility of our technique as related to the fabrication of human motion sensors, we attached five strain sensors to a latex glove to detect the joint bending motion, Figure 5a, b. The sensors were attached to the glove by bonding their ends to the glove using a cyanoacrylate adhesive (Loctite 420). Glove was subsequently donned and the bending angle (0–145°) of each finger at middle phalangeal joint was

DOI: 10.1021/am509087u
ACS Appl. Mater. Interfaces 2015, 7, 4463–4470

monitored by measuring the relative change in the resistance of the strain sensors. The tests were conducted performing a stepped bending sequence in which the fingers were bent and held for a few seconds at each position. Figure 5c shows the index finger at different bending angles and the time sequence of resistance change for two cycles ($R/R_o \approx 9$ for a completely bent joint).

To summarize, this work presents a low-cost and facile method for fabricating highly stretchable and sensitive carbon-based piezoresistive strain sensors. The fabrication is based on pyrolyzing conductive carbon patterns on the surface of a polyimide film using a CO_2 laser followed by its transfer to an elastomeric substrate. The carbonized material contain CNTs and multilayer graphene flakes that can be aligned in the direction of the laser scanning, imparting anisotropy (directionality) to the sensors not achievable using reported conductive nanocomposite methods.

■ ASSOCIATED CONTENT

Supporting Information

Additional figures (PDF). This material is available free of charge via the Internet at http://pubs.acs.org.

■ AUTHOR INFORMATION

Corresponding Author

*E-mail: bziaie@purdue.edu.

Notes

The authors declare no competing financial interest.

■ ACKNOWLEDGMENTS

The authors thank the staff of the Birck Nanotechnology Center for their support and assistance. Dr. Christopher Gilpin and the staff of the Purdue Multiscale Imaging Center's help in the TEM imaging is also greatly appreciated. Funding for this project was provided in part by the National Science Foundation under grant EFRI-BioFlex 1240443.

■ REFERENCES

(1) Mattmann, C.; Clemens, F.; Tröster, G. Sensor for Measuring Strain in Textile. *Sensors* **2008**, *8*, 3719−3732.

(2) Castano, L. M.; Flatau, A. B. Smart Fabric Sensors and E-Textile Technologies: A Review. *Smart Mater. Struct.* **2014**, *23*, 053001.

(3) Kim, R.-H.; Kim, D.-H.; Xiao, J.; Kim, B. H.; Park, S.-I.; Panilaitis, B.; Ghaffari, R.; Yao, J.; Li, M.; Liu, Z.; et al. Waterproof AlInGaP Optoelectronics on Stretchable Substrates with Applications in Biomedicine and Robotics. *Nat. Mater.* **2010**, *9*, 929−937.

(4) Kang, I.; Schulz, M. J.; Kim, J. H.; Shanov, V.; Shi, D. A Carbon Nanotube Strain Sensor for Structural Health Monitoring. *Smart Mater. Struct.* **2006**, *15*, 737−748.

(5) Scilingo, E. P.; Lorussi, F.; Mazzoldi, A.; De Rossi, D. Strain-Sensing Fabrics for Wearable Kinaesthetic-like Systems. *IEEE Sens. J.* **2003**, *3*, 460−467.

(6) Cai, L.; Song, L.; Luan, P.; Zhang, Q.; Zhang, N.; Gao, Q.; Zhao, D.; Zhang, X.; Tu, M.; Yang, F.; et al. Super-Stretchable, Transparent Carbon Nanotube-Based Capacitive Strain Sensors for Human Motion Detection. *Sci. Rep.* **2013**, *3*, 3048.

(7) Won, S. M.; Kim, H.-S.; Lu, N.; Kim, D.; Del Solar, C.; Duenas, T.; Ameen, A.; Rogers, J. A. Piezoresistive Strain Sensors and Multiplexed Arrays Using Assemblies of Single-Crystalline Silicon Nanoribbons on Plastic Substrates. *IEEE Trans. Electron Devices* **2011**, *58*, 4074−4078.

(8) Kim, Y.; Kim, Y.; Lee, C.; Kwon, S. Thin Polysilicon Gauge for Strain Measurement of Structural Elements. *IEEE Sens. J.* **2010**, *10*, 1320−1327.

(9) Yamada, T.; Hayamizu, Y.; Yamamoto, Y.; Yomogida, Y.; Izadi-Najafabadi, A.; Futaba, D. N.; Hata, K. A Stretchable Carbon Nanotube Strain Sensor for Human-Motion Detection. *Nat. Nanotechnol.* **2011**, *6*, 296−301.

(10) Lipomi, D. J.; Vosgueritchian, M.; Tee, B. C.-K.; Hellstrom, S. L.; Lee, J. a; Fox, C. H.; Bao, Z. Skin-like Pressure and Strain Sensors Based on Transparent Elastic Films of Carbon Nanotubes. *Nat. Nanotechnol.* **2011**, *6*, 788−792.

(11) Cohen, D. J.; Mitra, D.; Peterson, K.; Maharbiz, M. M. A Highly Elastic, Capacitive Strain Gauge Based on Percolating Nanotube Networks. *Nano Lett.* **2012**, *12*, 1821−1825.

(12) Park, J.; Wang, S.; Li, M.; Ahn, C.; Hyun, J. K.; Kim, D. S.; Kim, D. K.; Rogers, J. a; Huang, Y.; Jeon, S. Three-Dimensional Nanonetworks for Giant Stretchability in Dielectrics and Conductors. *Nat. Commun.* **2012**, *3*, 916.

(13) Cravanzola, S.; Haznedar, G.; Scarano, D.; Zecchina, A.; Cesano, F. Carbon-Based Piezoresistive Polymer Composites: Structure and Electrical Properties. *Carbon* **2013**, *62*, 270−277.

(14) Pyo, S.; Lee, J.-I.; Kim, M.-O.; Chung, T.; Oh, Y.; Lim, S.-C.; Park, J.; Kim, J. Development of a Flexible Three-Axis Tactile Sensor Based on Screen-Printed Carbon Nanotube-Polymer Composite. *J. Micromech. Microeng.* **2014**, *24*, 075012.

(15) Whitney, R. The Measurement of Volume Changes in Human Limbs. *J. Physiol* **1953**, *121*, 1−27.

(16) So, J.-H.; Thelen, J.; Qusba, A.; Hayes, G. J.; Lazzi, G.; Dickey, M. D. Reversibly Deformable and Mechanically Tunable Fluidic Antennas. *Adv. Funct. Mater.* **2009**, *19*, 3632−3637.

(17) Dickey, M. D.; Chiechi, R. C.; Larsen, R. J.; Weiss, E. a.; Weitz, D. a.; Whitesides, G. M. Eutectic Gallium-Indium (EGaIn): A Liquid Metal Alloy for the Formation of Stable Structures in Microchannels at Room Temperature. *Adv. Funct. Mater.* **2008**, *18*, 1097−1104.

(18) Muth, J. T.; Vogt, D. M.; Truby, R. L.; Mengüç, Y.; Kolesky, D. B.; Wood, R. J.; Lewis, J. a. Embedded 3D Printing of Strain Sensors within Highly Stretchable Elastomers. *Adv. Mater.* **2014**, 6307−6312.

(19) Raju, A. P. A.; Lewis, A.; Derby, B.; Young, R. J.; Kinloch, I. a.; Zan, R.; Novoselov, K. S. Wide-Area Strain Sensors Based upon Graphene-Polymer Composite Coatings Probed by Raman Spectroscopy. *Adv. Funct. Mater.* **2014**, *24*, 2865−2874.

(20) Kim, K. S.; Zhao, Y.; Jang, H.; Lee, S. Y.; Kim, J. M.; Kim, K. S.; Ahn, J.-H.; Kim, P.; Choi, J.-Y.; Hong, B. H. Large-Scale Pattern Growth of Graphene Films for Stretchable Transparent Electrodes. *Nature* **2009**, *457*, 706−710.

(21) Amjadi, M.; Pichitpajongkit, A.; Lee, S.; Ryu, S.; Park, I. Highly Stretchable and Sensitive Strain Sensor Based on Silver Nanowire-Elastomer Nanocomposite. *ACS Nano* **2014**, *8*, 5154−5163.

(22) Li, X.; Zhang, R.; Yu, W.; Wang, K.; Wei, J.; Wu, D.; Cao, A.; Li, Z.; Cheng, Y.; Zheng, Q.; et al. Stretchable and Highly Sensitive Graphene-on-Polymer Strain Sensors. *Sci. Rep.* **2012**, *2*, 870.

(23) Park, M.; Im, J.; Park, J.; Jeong, U. Micropatterned Stretchable Circuit and Strain Sensor Fabricated by Lithography on an Electrospun Nanofiber Mat. *ACS Appl. Mater. Interfaces* **2013**, *5*, 8766−8771.

(24) Lee, Y.; Bae, S.; Jang, H.; Jang, S.; Zhu, S.-E.; Sim, S. H.; Song, Y.; Il Hong, B. H.; Ahn, J.-H. Wafer-Scale Synthesis and Transfer of Graphene Films. *Nano Lett.* **2010**, *10*, 490−493.

(25) Lee, C.; Jug, L.; Meng, E. High Strain Biocompatible Polydimethylsiloxane-Based Conductive Graphene and Multiwalled Carbon Nanotube Nanocomposite Strain Sensors. *Appl. Phys. Lett.* **2013**, *102*, 183511.

(26) Hempel, M.; Nezich, D.; Kong, J.; Hofmann, M. A Novel Class of Strain Gauges Based on Layered Percolative Films of 2D Materials. *Nano Lett.* **2012**, *12*, 5714−5718.

(27) Correia, V.; Caparros, C.; Casellas, C.; Francesch, L.; Rocha, J. G.; Lanceros-Mendez, S. Development of Inkjet Printed Strain Sensors. *Smart Mater. Struct.* **2013**, *22*, 105028.

(28) Yao, S.; Zhu, Y. Wearable Multifunctional Sensors Using Printed Stretchable Conductors Made of Silver Nanowires. *Nanoscale* **2014**, *6*, 2345−2352.

DOI: 10.1021/am509087u
ACS Appl. Mater. Interfaces 2015, 7, 4463−4470

(29) Yan, C.; Wang, J.; Kang, W.; Cui, M.; Wang, X.; Foo, C. Y.; Chee, K. J.; Lee, P. S. Highly Stretchable Piezoresistive Graphene-Nanocellulose Nanopaper for Strain Sensors. *Adv. Mater.* **2014**, *26*, 2022−2027.
(30) Vinayan, B. P.; Nagar, R.; Raman, V.; Rajalakshmi, N.; Dhathathreyan, K. S.; Ramaprabhu, S. Synthesis of Graphene-Multiwalled Carbon Nanotubes Hybrid Nanostructure by Strengthened Electrostatic Interaction and Its Lithium Ion Battery Application. *J. Mater. Chem.* **2012**, *22*, 9949.
(31) Reina, A.; Jia, X.; Ho, J.; Nezich, D.; Son, H.; Bulovic, V.; Dresselhaus, M. S.; Kong, J. Large Area, Few-Layer Graphene Films on Arbitrary Substrates by Chemical Vapor Deposition. *Nano Lett.* **2009**, *9*, 30−35.
(32) Zhang, B.; Song, J.; Yang, G.; Han, B. Large-Scale Production of High-Quality Graphene Using Glucose and Ferric Chloride. *Chem. Sci.* **2014**, *5*, 4656−4660.

DOI: 10.1021/am509087u
ACS Appl. Mater. Interfaces 2015, 7, 4463−4470